

Blends of polythiophene nanowire/fluorine rubber with multiscale phase separation suitable for stretchable semiconductors



Yun-Chi Chiang^a, Chien-Chung Shih^a, Shih-Huang Tung^{b,c,*}, Wen-Chang Chen^{a,b,c,**}

^a Department of Chemical Engineering, National Taiwan University, Taipei, 10617, Taiwan

^b Institute of Polymer Science and Engineering, National Taiwan University, Taipei, 10617, Taiwan

^c Advanced Research Center for Green Materials Science and Technology, National Taiwan University, Taipei, 10617, Taiwan

HIGHLIGHTS

- The blending of P3HT with fluorine rubber creates stretchable semiconductors.
- The charge transporting and the stretchability of the films are both enhanced.
- The unique multiscale phase-separated structures contribute to the performance.

ARTICLE INFO

Keywords:

Polythiophene
Fluorine rubber
Phase separation
Stretchable organic field-effect transistor

ABSTRACT

We report an effective approach to prepare stretchable semiconductors by simply blending P3HT nanowires with fluorine rubber. The hole mobility of the field-effect transistors with the blend films as active layers is higher than that of pristine P3HT, and the mobility can maintain over $10^{-3} \text{ cm}^2 \text{ V}^{-1} \text{ s}^{-1}$ under 100% strain or even after 400 stretching/releasing cycles at 60% strain. The structures of the blend films were probed by TEM, AFM, X-ray diffraction, and polarized UV-vis spectrometry, which was then correlated to the electrical and the mechanical properties of the films. We find that because of the low miscibility between P3HT and fluorine rubber as well as the highly crystalline nature of P3HT, the blends phase separate into unique multiscale structures that can simultaneously enhance the charge transporting capability and the stretchability of the blend films.

1. Introduction

Polymeric semiconductors are emerging as a promising material for applications in wearable or deformable electronic devices due to their preferable mechanical resilience in comparison to their inorganic counterparts [1–7]. Numerous studies on stretchable thin film transistors using conjugated polymers as the active layer have been demonstrated [8–11]. Meanwhile, thanks to the substantial progress on the enhancement of carrier mobility in the past few years, conjugated polymers based thin film transistors show an ever-growing possibility for manufacturing of flexible and light-weight electronic devices as used in practice [12–21]. However, the conjugated polymers are rather stiff and brittle comparing to rubbers and plastic polymers [22–25]. Consequently, the mechanical instability of the electronic devices under applied tensile strain is inevitable. It is therefore importance to exploit high performance semiconductors with good mechanical durability able to endure high tensile deformation.

Unfortunately, efficient charge-transport in π -conjugated system strongly relies on their conjugated backbone with well-ordered intermolecular packing [20,26,27]. As known, high crystalline domains in a polymer matrix cause enhancement of film stiffness and brittleness because the rigid grain boundary restrict the strain release through the disordered polymer chains [24]. In this regard, some research groups have designed conjugated polymer with optimized alkyl chains or soft segments in the side chain position to meet the balance between incompatibility of crystallinity and ductility [13,28–31]. However, this approach usually accompanies a deterioration of charge mobility because the long side chains lead to less ordered packing and increase the amorphous regions, which results in inefficient delocalization of π -electrons.

An alternative approach to prepare stretchable semiconductors is to create elastomer/semiconductor blends [32]. The blending of conjugated polymers with insulated polymers have been widely investigated [33–36]. The vertical phase separation in a blend system is

* Corresponding author. Institute of Polymer Science and Engineering, National Taiwan University, Taipei, 10617, Taiwan.

** Corresponding author. Department of Chemical Engineering, National Taiwan University, Taipei, 10617, Taiwan.

E-mail addresses: shtung@ntu.edu.tw (S.-H. Tung), chenwc@ntu.edu.tw (W.-C. Chen).

thought to be necessary to maintain charge carrier mobility because it provides opportunity to form the continuous semiconducting layers [34]. In contrast, if semiconductors are well dispersed in the matrix or the blends form bulk heterojunction structures, the charge current density may be diminished due to the lack of continuous channels for charge transport, thus resulting in a poor mobility. By controlling solvent solubility, surface energy, and substrate wetting conditions, vertical phase separation can be induced during the solution casting process. Recently, several elastomer/conjugated polymer blends have been developed to enhance the endurance of semiconductors under strain [32,37–39]. Although the stretchability of the semiconductors is improved by incorporation of the elastomers, the charge carrier mobility is generally inferior to the pristine conjugated polymer due to the dilution effect. Hence, a new type of morphology in the elastomer/conjugated polymer blends with balanced electrical performance and mechanical properties is highly in demand [40].

Instead of vertical phase separation, we demonstrated in this study that the lateral phase separation of the blend films prepared simply by mixing P3HT with poly(vinylidene fluoride-hexafluoropropylene) (fluorine rubber) can induce local aggregated bundles of P3HT nanowires and create a suitable morphology for stretchable semiconductors. The fluorine rubber is an elastomer with a higher polarity than other common elastomers like PDMS and SEBS [41,42]. The low miscibility between P3HT and fluorine rubber, coupled with the crystallization of P3HT, cause the blends to be highly inhomogeneous, different from the previous studies using other rubbers that show dispersion of conjugated polymer nanofibrils in the rubber matrices [38,39]. The phase-separated structures, electric performances, and charge transport behaviors of the films under varying tensile strains were systematically investigated by TEM, AFM, GIWAXS/GISAXS, and UV-vis spectrometry. We report for the first time that the addition of fluorine rubber into P3HT can effectively improve both the electrical performance and mechanical stretchability of the blend films. The transistors with the blend films as active layers are demonstrated to be more capable of charge transport and more stretchable than those with pristine P3HT films. Such an improvement is closely correlated with the multiscale phase-separated structures in the P3HT/fluorine rubber blends.

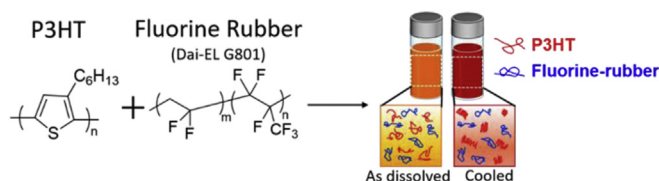
2. Experimental section

2.1. Materials

Poly(3-hexylthiophene-2,5-diyl) (M_w : 48k, PDI: 4.53) was purchased from Lumtec (Taiwan) and fluorine rubber (DAI-EL G-801) was purchased from Daikin (Japan), respectively. Anhydrous tetrahydrofuran (THF) was purchased from Sigma-Aldrich (U.S.A.). All the materials were used directly without further purification.

2.2. Sample preparation and structure characterization

To prepare the blend films with P3HT nanowires, P3HT and fluorine rubber were first dissolved in THF, a solvent of good miscibility with both P3HT and fluorine rubber. After completely dissolved, the solution was slowly cooled down to room temperature, and then stored in the refrigerator at 4 °C overnight, which facilitated the formation of self-assembled nanowires (Scheme 1). The solution exhibits brown color after the cooling process as shown in Fig. S1 of the Supporting Information. The blend films cast from the solutions were named as F_x -P3HT $_y$, where x is the concentration of fluorine rubber and y is the concentration of P3HT in the solutions, both in the unit of mg mL^{-1} . Transmission Electronic Microscope (TEM) images were collected by a JEOL 1230 at acceleration voltage set at 100 kV with thin films prepared on the carbon-supported grids. Surface morphology of thin films was probed by atomic force microscope (AFM) in tapping mode under ambient atmosphere via the Bruker, Innova system. The spring constant of the cantilevers (Nanosensor PPP-NCHR) was $\sim 42 \text{ N m}^{-1}$ and the



Scheme 1. Illustration of the preparation of P3HT and fluorine rubber blends. Temperature-dependent solubility was controlled to induce the self-assembly of P3HT chains into nanowires before film casting.

resonant frequency was $\sim 330 \text{ kHz}$. UV-vis absorption spectra were recorded on a Hitachi U-4100 spectrophotometer with the wavelength range from 300 to 800 nm. For polarized UV-vis spectroscopy, a rotational polarizer was introduced to measure the absorption with the polarized incident light parallel or perpendicular to the stretching direction. The dichroic ratio (R) of thin films were calculated as $R = A_{\parallel}/A_{\perp}$, where A is the absorption intensity at 555 nm. Grazing-incident small-angle and wide-angle X-Ray scattering (GISAXS and GIWAXS) for thin films were carried out on beamline 23A1 and beamline 13A1 in National Synchrotron Radiation Research Center (NSRRC), Taiwan, with monochromatic beams of wavelength $\lambda = 0.82656 \text{ \AA}$ and 1.0227 \AA , respectively. The incident angle was set at 0.12° for both experiments and the scattering intensities are reported as intensity versus q , where $q = (4\pi/\lambda) \times \sin(\theta/2)$ and θ is the scattering angle.

2.3. Fabrication and characterization of field-effect transistors

Field-effect transistors were fabricated with a bottom-gate/top-contact configuration. A 300 nm SiO_2 layer with capacitance per unit area = 10 nF cm^{-2} as gate dielectric was thermally grown onto the highly n-type doped Si (100) substrates. The substrates were modified with an octadecyltrimethoxysilane (ODTS) self-assembled monolayer according to the reported method [43]. The polymer thin films were spin-coated onto modified SiO_2/Si substrates, and a post-annealing process at 150 °C under vacuum for 30 min was consequently introduced to promote the molecular packing that enhances the resultant FET performance. The top-contact source/drain gold electrodes with thickness of 65 nm were thermally evaporated through a regular shadow mask, with the channel length (L) and width (W) being 50 and 1000 μm , respectively. For the measurements of the electrical characteristics of the stretched thin films, the thin films were spin-cast on ODTS-modified silicon substrate first, followed by transferred onto PDMS slabs (15:1 base to cross-linker by mass ratio) where the films are stretched to desired strain level. The stretched thin films were transferred again from PDMS slabs back onto silicon substrates for transistor fabrication and characterization.

3. Results and discussion

3.1. Phase-separated structures of blend films

P3HT nanowires and their distributions in thin films before and after blending with fluorine rubber were observed by TEM. In the case of pristine P3HT (Fig. 1a), the TEM image shows randomly distributed nanowires with lengths around several hundred nanometers. After blending with fluorine rubber at a weight ratio of 1:4 (F_1 -P3HT $_4$), the fluorine rubber-rich phases with lower electron density form the light, round domains randomly dispersed in the matrix consisting of bundled P3HT nanowires (Fig. 1b). The P3HT-rich domains remain continuous throughout the sample even when the weight fraction of fluorine rubber increases to be equal to that of P3HT, as shown in Fig. 1c for F_4 -P3HT $_4$ film. The smaller black circular domains that generally locate on the edges of the light areas (Fig. 1b and c) should also be the fluorine rubber-rich phases but with larger film thickness, which are formed possibly due to the dewetting of the solution during solvent

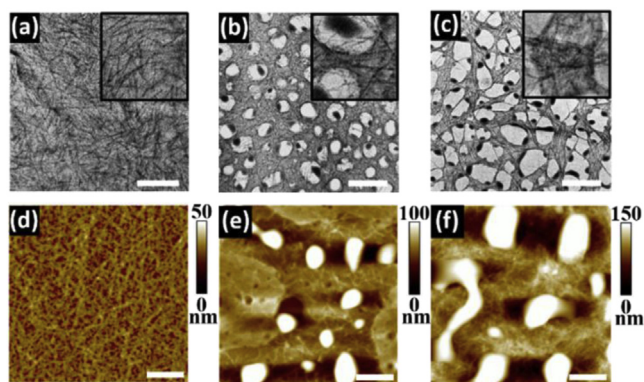


Fig. 1. TEM images of (a) pristine P3HT, (b) F₁-P3HT₄, and (c) F₄-P3HT₄ (inset: 500 × 500 nm), and tapping mode AFM topographies of (d) pristine P3HT, (e) F₁-P3HT₄, and (f) F₄-P3HT₄. The scale bar is 1 μm.

evaporation. The long P3HT nanowires are confined in the narrow, continuous P3HT-rich domains, which forces the high-aspect-ratio nanowires to align in a higher local orientational order due to the excluded volume effect [44]. The alignment of the P3HT nanowires in the limited spaces results in a denser spatial distribution of the nanowires. In other words, the inter-distance between the P3HT nanowires decreases to form the bundles after blending with fluorine rubber. This self-confined behavior is attributed to the large-scale phase separation caused by the low miscibility between fluorine rubber and P3HT.

The corresponding surface morphology on silicon wafer were further investigated by AFM. The topography and phase images of the blend thin films are presented in Fig. 1d–f and Fig. S2, respectively. While the pristine P3HT shows intertwined nanowires that cover the whole surface area, the blend films reveal the rubber-rich domains with higher altitude spreading on the surface and the domains grow as the fraction of rubber increases. Similar to the TEM images, the AFM results suggest that in the blend thin films, P3HT and fluorine rubber phase separate into isolated rubber-rich domains distributed in continuous P3HT-rich phases. This unique phase separation structure is considered as the promising feature for enhancing not only the charge-transporting capability but also the mechanical resilience of the blend films.

The nanoscale structures of the blend thin films were elucidated by grazing incident small-angle X-ray scattering (GISAXS) analyses. As presented in Fig. 2a, the scattering intensity of pristine P3HT and fluorine rubber decrease monotonically with increasing wave vector q

and no apparent structural information were observed from the profile. In contrast, F₁-P3HT₄ and F₄-P3HT₄ blend thin films show scattering shoulders between $q = 0.015$ to 0.03 \AA^{-1} and the shoulder becomes more pronounced for F₄-P3HT₄. Similar scattering profiles have been reported in P3HT/PCBM blend systems where the shoulders have been demonstrated to be given by the P3HT crystallites ($\sim 15 \text{ nm}$ in size) surrounded by P3HT/PCBM intermixed amorphous phases [45–48]. The absence of the shoulder for pristine P3HT is due to the lack of electron density contrast between crystalline P3HT and amorphous P3HT. In the blends, a small amount of rubber may mix with the amorphous P3HT in the P3HT-rich domains, therefore enhancing the electron density contrast between P3HT crystallites and the rubber/amorphous P3HT intermixed phases due to the lower electron density of the rubber. This explains why the scattering shoulders appear. Thus, in addition to the formation of rubber-rich and P3HT-rich domains observed from TEM and AFM, the GISAXS results further reveal the existence of the rubber/amorphous P3HT intermixed phases in the P3HT-rich domains, which is believed advantageous to the stretchability of the blend films.

Fig. 2b shows the UV-vis absorption spectra of the films. All the curves are essentially overlapped and the common absorption peaks are at 520, 555 and 605 nm, indicating that the blending of fluorine rubber in P3HT does not change the absorption. It is well known that regioregular P3HT is capable of forming crystals due to their highly ordered chain configuration and the thermodynamically-preferred planar chain conformation. In the P3HT crystallites, the high degree intra-chain ordering increases the conjugation length and causes the absorption peak around 555 nm while the inter-chain π - π stacking leads to the absorption around 605 nm. Thus, the addition of the fluorine rubber does not affect the chain conformation and chain packing of P3HT, which implies that the rubber is excluded from the P3HT crystallites. Apart from the crystalline regions, the peak at lower wavelength, 520 nm, is attributed to the less ordered P3HT chains in the amorphous regions restrained by P3HT crystallites [49,50]. The molecular packing of P3HT chains were examined by 2-D GIWAXS as shown in Fig. 2c and the scans along q_z and q_y directions are shown in Fig. S3. Both pristine P3HT and blend thin films exhibit well-ordered edge-on stacking with similar diffraction signals in the out-of-plane direction (along q_z axis) and in-plane direction (along q_y axis). The similar lamellar spacing (around 16.41–16.49 Å) and the π - π stacking spacing (3.79–3.85 Å) estimated from the diffraction spots again indicate that the fluorine rubber is unable to interfere with the packing of P3HT chains, consistent with the UV-vis measurements, due to the crystallization-induced phase separation that repel the fluorine rubber out of the close-packing region of P3HT.

By combining the results of the imaging, scattering, and absorption spectrum, the phase separations in the blend thin films can be classified into two main scales: (i) the large-scaled separation of fluorine rubber-rich and P3HT-rich domains, and (ii) the small-scaled pure P3HT crystallites separated from the rubber/amorphous P3HT intermixed phases in the P3HT-rich domains. The P3HT crystallites form the nanowires that are closely aligned in the continuous P3HT-rich domains, providing a preferable channel to transport the charge carriers. The fluorine rubber-rich domains and the rubber/amorphous P3HT intermixed phases in the P3HT-rich domains are the flexible regions that can effectively bear the stress when thin films are under tensile strains. Such a structure allows the blend thin films to achieve both mechanical resilience and charge transport.

3.2. Morphology of blend films under stretching

For the characterizations of the stretched thin films under different strain levels, the transfer method was introduced, as shown in Fig. 3a. The blend films were transferred onto an elastomeric PDMS slabs and the tensile strains were applied to the PDMS slabs such that the thin films were stretched accordingly. The stretched thin films were used

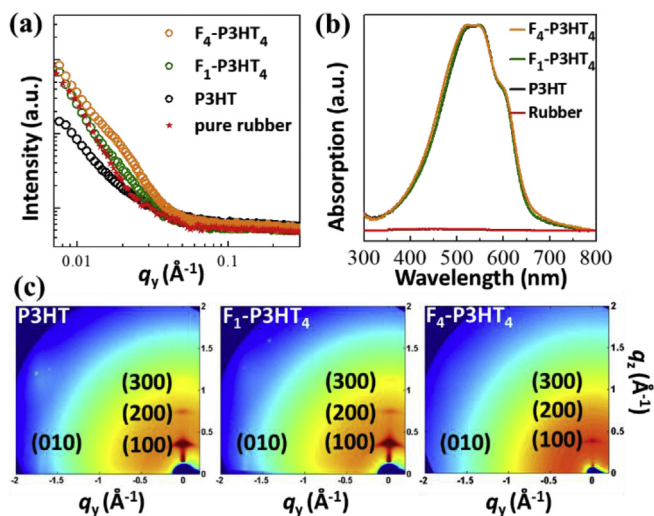


Fig. 2. (a) GISAXS profiles from q_y scan at $q_z = 0.027 \text{ \AA}^{-1}$, (b) UV-vis absorption spectra, and (c) 2-D GIWAXS patterns of the pristine P3HT and the blend thin films.

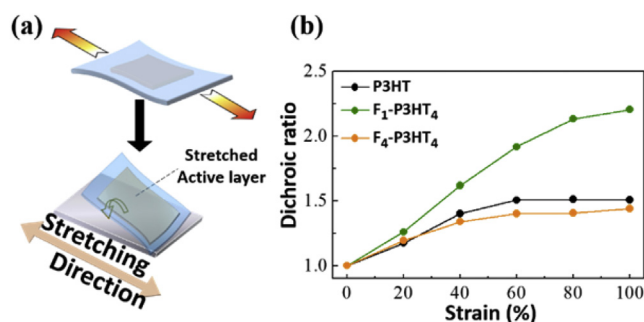


Fig. 3. (a) Schematic illustration of preparing stretched polymer thin films through transfer method. (b) Dichroic ratio (R) of the pristine P3HT and the blend films.

directly or transferred back onto the silicon substrates for the characterizations. The orientation of P3HT chains in thin films under varying strains was measured by polarized UV-vis spectroscopy. The data are shown in Fig. S4. The corresponding dichroic ratios (R) were calculated based on the absorption intensity at 555 nm. As shown in Fig. 3b, the R values of pristine P3HT and F₄-P3HT₄ change similarly with strain, progressively increasing to 1.3–1.4 as the strain level increases from 0% to 40% and then remaining constant around 1.4–1.5 at strains higher than 60%. In the case of F₁-P3HT₄ film, the R value keeps increasing to around 2.2 at 100% strain, implying a higher degree of orientation for the stretched film. The results suggest that the orientation of P3HT chains upon stretching could be enhanced by the addition of a proper amount of fluorine rubber.

The surface morphologies of the stretched thin films were explored by AFM as shown in Fig. 4. Clear cracks with long axis perpendicular to the stretching direction are observed on the pristine P3HT thin films at 60% strain, while for the blend thin film, F₁-P3HT₄, the cracks are barely seen at this strain level. This evidences the improvement on the stretchability of the blend thin films. The propagation of cracks is effectively suppressed via the deformation of the flexible rubber-rich domains and the rubber/amorphous P3HT intermixed phases. At the strain level up to 100%, micro-scale cracks appear in all the thin films. The formation of cracks is an indication of the breakdown of the continuous channel for charge transport, which is responsible for the lower charge carrier mobilities of the stretched films, as discussed later.

The molecular stacking of P3HT in the films under strain was further investigated through the GIWAXS technique, shown in Fig. S5 and S6. The incident X-ray beam was set to be parallel or perpendicular to the stretching direction. As shown in Fig. 5, the lamellar spacing of pristine P3HT, F₁-P3HT₄, and F₄-P3HT₄ are initially 16.49 Å, 16.41 Å, and 16.41 Å, respectively. When the strain increases from 0% to 40%, the spacing of pristine P3HT decreases to a minimum of 15.85 Å at 40% strain in both directions, corresponding to a 3.88% drop. Although the lamellar spacing of the blend films also shows the minima at 40% strain, 16.01 Å and 16.11 Å for F₁-P3HT₄ and F₄-P3HT₄ respectively,

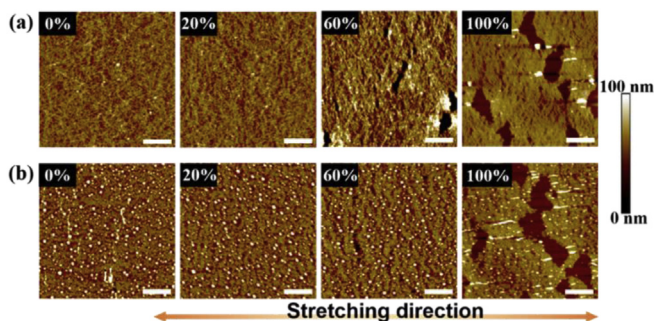


Fig. 4. AFM topographies of (a) pristine P3HT and (b) F₁-P3HT₄ blend thin films under varying tensile strains. The scale bar is 2 μm.

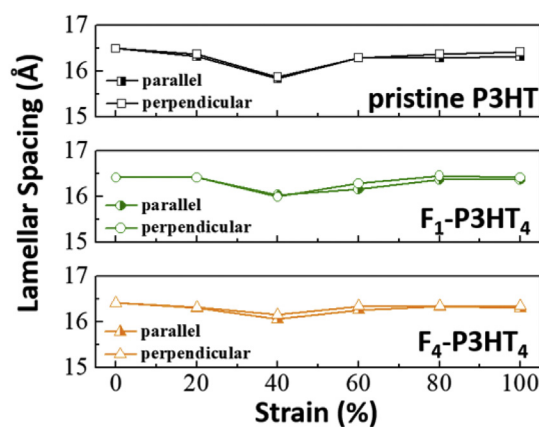


Fig. 5. Lamellar spacing of pristine P3HT, F₁-P3HT₄, and F₄-P3HT₄ thin films under varying strains. The incident X-ray beam is set to be perpendicular or parallel to the stretching direction.

the drops are not as high as that of pristine P3HT, only 2.44% and 1.83%. The decrease in spacing is possibly due to the compression in the direction of lamellar stacking to maintain the sample volumes when the films are stretched. As more rubber is added into P3HT, the flexible rubber bears more deformation and thus the P3HT lamellae is less compressed, which manifests the more stretchable behavior for the blend films. When the strain is increased from 40% to 100%, the lamellar spacing of all the films turn back approximately to their original values. This could be attributed to the crack formation that releases local stress above 40% strain, in agreement with the AFM observation on the stretched films.

3.3. Electrical properties of FETs

To examine the effect of the blended fluorine rubber on the charge-transporting behavior of P3HT, we fabricated FETs devices through the transfer method as shown in Fig. 6a and a detailed preparation process is illustrated in Fig. S7. Electrical properties in both perpendicular and parallel directions relative to the stretching direction with strains of 0–100% were measured. The transfer curves, i.e. drain current I_{ds} vs gate voltage V_g , are shown in Fig. 6b and the corresponding electrical details are summarized in Table 1. The charge carrier mobilities were calculated from the gate voltage range between -30 V and -50 V, where the $I_{ds}^{1/2}$ vs. V_g curves show good linearity, as exemplified in Fig. S8. The averaged carrier mobilities of the unstrained pristine P3HT, F₁-P3HT₄ and F₄-P3HT₄ based field-effect transistors are 4.2×10^{-3} , 1.1×10^{-2} , and $7.3 \times 10^{-3} \text{ cm}^2 \text{ V}^{-1} \text{ s}^{-1}$, respectively. With the fluorine rubber blended, the mobility is significantly improved in comparison to that of the pristine P3HT, especially for F₁-P3HT₄, which could be ascribed to the locally aligned P3HT bundles in the continuous P3HT-rich domains that reduce the charge transport barriers. Because of the intrinsically insulated property of fluorine rubber, excess rubber may have a negative effect on the charge transport. This explains why the device with higher fraction of rubber, F₄-P3HT₄, exhibits a lower mobility than that with F₁-P3HT₄.

The strain-dependent electrical properties of the transistors up to 100% strain are shown in Fig. 6c and Fig. S9. The mobilities of the pristine P3HT device parallel and perpendicular to the stretching direction show similar trends, continuously decreasing from 4.2×10^{-3} at 0% strain to 6.0×10^{-4} and $5.4 \times 10^{-4} \text{ cm}^2 \text{ V}^{-1} \text{ s}^{-1}$ at 100% strain, respectively. In contrast, for the F₁-P3HT₄ device, the mobilities can be well maintained till 60% strain and then decrease to 2.3×10^{-3} and $2.0 \times 10^{-3} \text{ cm}^2 \text{ V}^{-1} \text{ s}^{-1}$ at 100% strain in parallel and perpendicular directions, both showing less drops than the pristine P3HT device. The results are consistent with the dependence of the crack formation on strain shown in the AFM images of Fig. 4 where the

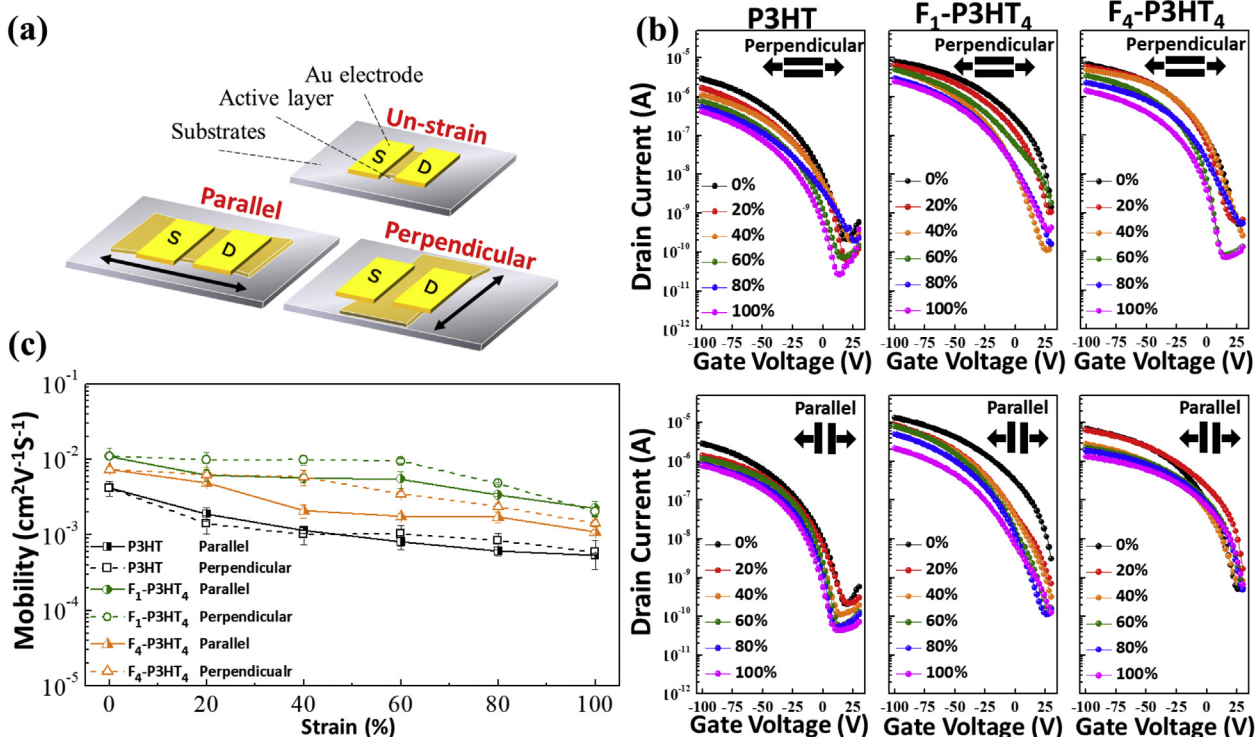


Fig. 6. (a) Schematic illustration of the FETs with the charge-transferring direction parallel or perpendicular to the stretching direction. (b) Transfer characteristics of the pristine P3HT, F₁-P3HT₄, and F₄-P3HT₄-based FETs measured in perpendicular and parallel direction under varying tensile strains. (c) Charge carrier mobility of the FETs as functions of strain. The source-to-drain voltage was -100 V.

cracks in F₁-P3HT₄ film are nearly invisible even at 60% strain. The transistor based on F₄-P3HT₄ also shows an improvement on the charge transport against stretching in the two directions compared to pristine P3HT, from 7.3×10^{-3} to 1.1×10^{-3} and $1.4 \times 10^{-3} \text{ cm}^2 \text{ V}^{-1} \text{ s}^{-1}$ at 100% strain. Therefore, the blending of fluorine rubber into P3HT as active layers not only increases the charge carrier mobility but also effectively prevents the mobility from decay as the films are strained. The output characteristics are shown in Fig. S10 where a good current modulation can be observed. The devices based on F₁-P3HT₄ were further examined for a 400 stretching/releasing cycling test with the strain level set at 40% and 60% (Fig. 7, S11, and S12). At both strain levels, the mobilities of the devices initially decrease and then reach nearly constant values after 200 cycle times, around 3.0×10^{-3} and $1.1 \times 10^{-3} \text{ cm}^2 \text{ V}^{-1} \text{ s}^{-1}$, respectively, which manifests a good operating stability for the stretchable active layer.

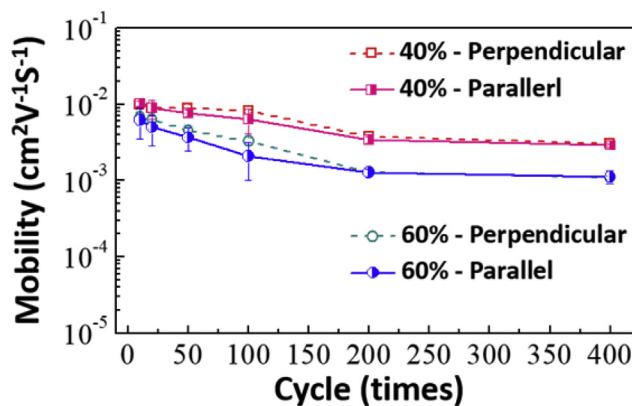


Fig. 7. Dependence of the charge carrier mobility on stretching/relaxing cycles under 40% and 60% strain for F₁-P3HT₄-based FET devices measured in perpendicular and parallel direction.

Table 1
Detailed FET electrical characteristics of the polymer blend thin films.

Strain	Stretching Direction	Pristine P3HT			F ₁ -P3HT ₄			F ₄ -P3HT ₄		
		μ ($\text{cm}^2 \text{ V}^{-1} \text{ s}^{-1}$)	$I_{\text{on}}/I_{\text{off}}$	V_{th} (V)	μ ($\text{cm}^2 \text{ V}^{-1} \text{ s}^{-1}$)	$I_{\text{on}}/I_{\text{off}}$	V_{th} (V)	μ ($\text{cm}^2 \text{ V}^{-1} \text{ s}^{-1}$)	$I_{\text{on}}/I_{\text{off}}$	V_{th} (V)
0	–	4.2×10^{-3}	$\sim 10^4$	–8	1.1×10^{-2}	$\sim 10^4$	13	7.3×10^{-3}	$\sim 10^4$	16
20	parallel	1.4×10^{-3}	$\sim 10^4$	–1	6.3×10^{-3}	$\sim 10^4$	4	4.9×10^{-3}	$\sim 10^4$	15
	perpendicular	1.9×10^{-3}	$\sim 10^4$	–7	9.9×10^{-3}	$\sim 10^4$	7	6.3×10^{-3}	$\sim 10^4$	13
40	parallel	1.0×10^{-3}	$\sim 10^4$	–1	5.6×10^{-3}	$\sim 10^4$	0	2.1×10^{-3}	$\sim 10^4$	17
	perpendicular	1.2×10^{-3}	$\sim 10^4$	–5	9.8×10^{-3}	$\sim 10^4$	3	5.8×10^{-3}	$\sim 10^4$	10
60	parallel	1.0×10^{-3}	$\sim 10^4$	0	5.5×10^{-3}	$\sim 10^4$	–3	1.8×10^{-3}	$\sim 10^4$	14
	perpendicular	8.1×10^{-4}	$\sim 10^4$	–9	9.5×10^{-3}	$\sim 10^4$	–1	3.5×10^{-3}	$\sim 10^4$	7
80	parallel	8.4×10^{-4}	$\sim 10^4$	–2	3.4×10^{-3}	$\sim 10^4$	–6	1.7×10^{-3}	$\sim 10^4$	13
	perpendicular	6.1×10^{-4}	$\sim 10^4$	–8	4.8×10^{-3}	$\sim 10^4$	–3	2.4×10^{-3}	$\sim 10^4$	9
100	parallel	6.0×10^{-4}	$\sim 10^4$	–6	2.3×10^{-3}	$\sim 10^4$	–6	1.1×10^{-3}	$\sim 10^4$	14
	perpendicular	5.4×10^{-4}	$\sim 10^4$	–11	2.0×10^{-3}	$\sim 10^4$	–4	1.4×10^{-3}	$\sim 10^4$	8

4. Conclusion

We have demonstrated a stretchable semiconductor formed by blends of P3HT nanowires and fluorine rubber, where the multiscale phase separation happens to meet the requirements of stretchable semiconductors. The low miscibility between P3HT and fluorine rubber leads to the formation of continuous P3HT-rich domains and randomly distributed fluorine rubber-rich domains in the blends. The long P3HT nanowires are confined in the narrow P3HT-rich domains and tend to closely align to facilitate charge transport. The charge carrier mobility of the blend film as active layers in transistors is thus higher than that of pristine P3HT. Furthermore, in the P3HT-rich domains, apart from the P3HT crystallites that organize into nanowires, the amorphous P3HT mixes with fluorine rubber to form the rubber/amorphous P3HT intermixed phases. The flexible fluorine rubber-rich domains along with the intermixed phases impart the stretchability to the blend films, and therefore the charge carrier mobility can be effectively maintained when the films are stretched. This work provides a simple method to simultaneously enhance the charge transporting capability and the stretchability of the organic semiconductors that are potential to be integrated into wearable electronics.

Acknowledgements

This work was financially supported by the “Advanced Research Center of Green Materials Science and Technology” from The Featured Area Research Center Program within the framework of the Higher Education Sprout Project by the Ministry of Education (107L9006) and the Ministry of Science and Technology in Taiwan (MOST 106-2218-E-002-021-MY2 & 107-3017-F-002-001). The authors also acknowledge National Synchrotron Radiation Research Center, Taiwan, for facilitating the X-ray scattering experiments.

Appendix A. Supplementary data

Supplementary data to this article can be found online at <https://doi.org/10.1016/j.polymer.2018.09.044>.

References

- [1] S. Savagatrup, A.D. Printz, T.F. O'Connor, A.V. Zaretski, D.J. Lipomi, *Chem. Mater.* 26 (2014) 3028–3041.
- [2] S.E. Root, S. Savagatrup, A.D. Printz, D. Rodriguez, D.J. Lipomi, *Chem. Rev.* 117 (2017) 6467–6499.
- [3] D.J. Lipomi, B.C.K. Tee, M. Vosgueritchian, Z. Bao, *Adv. Mater.* 23 (2011) 1771–1775.
- [4] D.J. Lipomi, B.C.K. Tee, M. Vosgueritchian, Z. Bao, *Adv. Mater.* 26 (2014) 4253–4259.
- [5] C.-C. Shih, W.-Y. Lee, C. Lu, H.-C. Wu, W.-C. Chen, *Adv. Electron. Mater.* 3 (2017) 1600477.
- [6] J.Y. Oh, S. Rondeau-Gagné, Y.-C. Chiu, A. Chortos, F. Lissel, G.-J.N. Wang, B.C. Schroeder, T. Kurosawa, J. Lopez, T. Katsumata, J. Xu, C. Zhu, X. Gu, W.-G. Bae, Y. Kim, L. Jin, J.W. Chung, J.B.H. Tok, Z. Bao, *Nature* 539 (2016) 411.
- [7] Y. Qian, X. Zhang, L. Xie, D. Qi, B.K. Chandran, X. Chen, W. Huang, *Adv. Mater.* 28 (2016) 9243–9265.
- [8] H.-F. Wen, H.-C. Wu, J. Aimi, C.-C. Hung, Y.-C. Chiang, C.-C. Kuo, W.-C. Chen, *Macromolecules* 50 (2017) 4982–4992.
- [9] J.-T. Wang, S. Takshima, H.-C. Wu, C.-C. Shih, T. Isono, T. Kakuchi, T. Satoh, W.-C. Chen, *Macromolecules* 50 (2017) 1442–1452.
- [10] M. Shin, J.H. Song, G.-H. Lim, B. Lim, J.-J. Park, U. Jeong, *Adv. Mater.* 26 (2014) 3706–3711.
- [11] Y. Yao, H. Dong, W. Hu, *Adv. Mater.* 28 (2016) 4513–4523.
- [12] H. Luo, C. Yu, Z. Liu, G. Zhang, H. Geng, Y. Yi, K. Broch, Y. Hu, A. Sadhanala, L. Jiang, P. Qi, Z. Cai, H. Sirringhaus, D. Zhang, *Sci. Adv.* 2 (2016) e1600076.
- [13] A.F. Paterson, N.D. Treat, W. Zhang, Z. Fei, G. Wyatt-Moon, H. Faber, G. Vourlias, P.A. Patsalas, O. Solomeshch, N. Tessler, M. Heeney, T.D. Anthopoulos, *Adv. Mater.* 28 (2016) 7791–7798.
- [14] S.R. Forrest, *Nature* 428 (2004) 911–918.
- [15] H.N. Tsao, D.M. Cho, I. Park, M.R. Hansen, A. Mavrinskiy, D.Y. Yoon, R. Graf, W. Pisula, H.W. Spiess, K. Müllen, *J. Am. Chem. Soc.* 133 (2011) 2605–2612.
- [16] B. Nketia-Yawson, H.-S. Lee, D. Seo, Y. Yoon, W.-T. Park, K. Kwak, H.J. Son, B. Kim, Y.-Y. Noh, *Adv. Mater.* 27 (2015) 3045–3052.
- [17] Tao Xie, Guangzhong Xie, Hongfei Du, Yuanjie Su, Zongbiao Ye, Yuyan Chen, Yadong Jiang, *Sensor. Actuator. B* 230 (2016) 176–183.
- [18] Tao Xie, Guangzhong Xie, Yuanjie Su, Hongfei Du, Zongbiao Ye, Yadong Jiang, *Nanotechnology* 27 (2016) 065502.
- [19] Yuanjie Su, Guangzhong Xie, Huiling Tai, Shuangding Li, Boxi Yang, Si Wang, Qiuping Zhang, Hongfei Du, Hulin Zhang, Xiaosong Du, Yadong Jiang, *Nano Energy* 47 (2018) 316–324.
- [20] Yuanjie Su, Guangzhong Xie, Si Wang, Huiling Tai, Qiuping Zhang, Hongfei Du, Hulin Zhang, Xiaosong Du, Yadong Jiang, *Sensor. Actuator. B* 251 (2017) 144–152.
- [21] Yuanjie Su, Guangzhong Xie, Jun Chen, Hongfei Du, Hulin Zhang, Zhen Yuan, Zongbiao Ye, Xiaosong Du, Huiling Tai, Yadong Jiang, *RSC Adv.* 6 (2016) 97840–97847.
- [22] H.-C. Wu, S.J. Benight, A. Chortos, W.-Y. Lee, J. Mei, J.W.F. To, C. Lu, M. He, J.B.H. Tok, W.-C. Chen, Z. Bao, *Chem. Mater.* 26 (2014) 4544–4551.
- [23] Y. Lee, M. Shin, K. Thiagarajan, U. Jeong, *Macromolecules* 49 (2016) 433–444.
- [24] H.J. Kim, M.Y. Lee, J.-S. Kim, J.-H. Kim, H. Yu, H. Yun, K. Liao, T.-S. Kim, J.H. Oh, B.J. Kim, *ACS Appl. Mater. Interfaces* 9 (2017) 14120–14128.
- [25] J.I. Scott, X. Xue, M. Wang, R.J. Kline, B.C. Hoffman, D. Dougherty, C. Zhou, G. Bazan, B.T. O'Connor, *ACS Appl. Mater. Interfaces* 8 (2016) 14037–14045.
- [26] R. Noriega, J. Rivnay, K. Vandewal, F.P.V. Koch, N. Stingelin, P. Smith, M.F. Toney, A. Salleo, *Nat. Mater.* 12 (2013) 1038–1044.
- [27] H. Sirringhaus, M. Bird, N. Zhao, *Adv. Mater.* 22 (2010) 3893–3898.
- [28] S. Savagatrup, A.D. Printz, T.F. O'Connor, A.V. Zaretski, D. Rodriguez, E.J. Sawyer, K.M. Rajan, R.I. Acosta, S.E. Root, D.J. Lipomi, *Energy Environ. Sci.* 8 (2015) 55–80.
- [29] S. Savagatrup, A.S. Makaram, D.J. Burke, D.J. Lipomi, *Adv. Funct. Mater.* 24 (2014) 1169–1181.
- [30] S. Savagatrup, A.D. Printz, D. Rodriguez, D.J. Lipomi, *Macromolecules* 47 (2014) 1981–1992. *Macromolecules* 47 (2014) 1981–1992.
- [31] C. Lu, W.-Y. Lee, X. Gu, J. Xu, H.-H. Chou, H. Yan, Y.-C. Chiu, M. He, J.R. Matthews, W. Niu, J.B.H. Tok, M.F. Toney, W.-C. Chen, Z. Bao, *Adv. Electron. Mater.* 3 (2017) 1600311.
- [32] J. Xu, S. Wang, G.-J.N. Wang, C. Zhu, S. Luo, L. Jin, X. Gu, S. Chen, V.R. Feig, J.W.F. To, S. Rondeau-Gagné, J. Park, B.C. Schroeder, C. Lu, J.Y. Oh, Y. Wang, Y.-H. Kim, H. Yan, R. Sinclair, D. Zhou, G. Xue, B. Murmann, C. Linder, W. Cai, J.B.H. Tok, J.W. Chung, Z. Bao, *Science* 355 (2017) 59–64.
- [33] X. Wang, W.H. Lee, G. Zhang, X. Wang, B. Kang, H. Lu, L. Qiu, K. Cho, *J. Mater. Chem. C* 1 (2013) 3989–3998.
- [34] L. Qiu, J.A. Lim, X. Wang, W.H. Lee, M. Hwang, K. Cho, *Adv. Mater.* 20 (2008) 1141–1145.
- [35] A. Babel, S.A. Jenekhe, *Macromolecules* 37 (2004) 9835–9840.
- [36] L. Qiu, W.H. Lee, X. Wang, J.S. Kim, J.A. Lim, D. Kwak, S. Lee, K. Cho, *Adv. Mater.* 21 (2009) 1349–1353.
- [37] B. Kang, F. Ge, L. Qiu, K. Cho, *Adv. Electron. Mater.* 3 (2017) 1600240.
- [38] M. Shin, J.Y. Oh, K.-E. Byun, Y.-J. Lee, B. Kim, H.-K. Baik, J.-J. Park, U. Jeong, *Adv. Mater.* 27 (2015) 1255–1261.
- [39] D. Choi, H. Kim, N. Persson, P.-H. Chu, M. Chang, J.-H. Kang, S. Graham, E. Reichmanis, *Chem. Mater.* 28 (2016) 1196–1204.
- [40] T. Sun, J.I. Scott, M. Wang, R.J. Kline, G.C. Bazan, B.T. O'Connor, *Adv. Electron. Mater.* 3 (2017) 1600388.
- [41] C. Lu, W.-Y. Lee, C.-C. Shih, M.-Y. Wen, W.-C. Chen, *ACS Appl. Mater. Interfaces* 9 (2017) 25522–25532.
- [42] D. Kong, R. Pfattner, A. Chortos, C. Lu, A.C. Hincley, C. Wang, W.-Y. Lee, J.W. Chung, Z. Bao, *Adv. Funct. Mater.* 26 (2016) 4680–4686.
- [43] Y. Ito, A.A. Virkar, S. Mannsfeld, J.H. Oh, M. Toney, J. Locklin, Z. Bao, *J. Am. Chem. Soc.* 131 (2009) 9396–9404.
- [44] D. Frenkel, *Liq. Cryst.* 5 (1989) 929–940.
- [45] P. Kohn, Z. Rong, K.H. Scherer, A. Sepe, M. Sommer, P. Müller-Buschbaum, R.H. Friend, U. Steiner, S. Hüttner, *Macromolecules* 46 (2013) 4002–4013.
- [46] C.-H. Liu, W.-H. Tseng, C.-Y. Cheng, C.-I. Wu, P.-T. Chou, S.-H. Tung, *J. Polym. Sci., Part B: Polym. Phys.* 54 (2016) 975–985.
- [47] W.-R. Wu, U.S. Jeng, C.-J. Su, K.-H. Wei, M.-S. Su, M.-Y. Chiu, C.-Y. Chen, W.-B. Su, C.-H. Su, A.-C. Su, *ACS Nano* 5 (2011) 6233–6243.
- [48] C.-Y. Chen, C.-S. Tsao, Y.-C. Huang, H.-W. Liu, W.-Y. Chiu, C.-M. Chuang, U.S. Jeng, C.-J. Su, W.-R. Wu, W.-F. Su, L. Wang, *Nanoscale* 5 (2013) 7629–7638.
- [49] J. Clark, J.-F. Chang, F.C. Spano, R.H. Friend, C. Silva, *Appl. Phys. Lett.* 94 (2009) 163306.
- [50] P.J. Brown, D.S. Thomas, A. Köhler, J.S. Wilson, J.-S. Kim, C.M. Ramsdale, H. Sirringhaus, R.H. Friend, *Phys. Rev. B* 67 (2003) 064203.